Canadian Science Publishing
NRC Research Press journals | Publishing Services

Canadian Geotechnical Journal
Revue canadienne de géotechnique

Collapsibility, composition, and microstructure of a loess in China

Journal:	*Canadian Geotechnical Journal*
Manuscript ID	cgj-2015-0285.R1
Manuscript Type:	Article
Date Submitted by the Author:	29-Sep-2015
Complete List of Authors:	Liu, Zhen; Louisiana State University, Department of Civil and Environmental Engineering Liu, Fengyin; Xi'an University of Technology, School of Civil Engineering and Architecture Ma, Fuli; Taiyuan University of Technology, College of Architecture and Civil Engineering Wang, Mei; Taiyuan University of Technology, College of Architecture and Civil Engineering Bai, Xiaohong; Taiyuan University of Technology, College of Architecture and Civil Engineering Zheng, Yonglai; Tongji University, Department of Hydraulic Engineering Yin, Hang; Louisiana State University, Department of Civil and Environmental Engineering Zhang, Guoping; University of Massachusetts Amherst, Civil & Environmental Eng.
Keyword:	Collapsibility, Loess, Microstructure, Mineralogy, Particle morphology

First version, June 2015

Revision, September 2015

Collapsibility, composition, and microstructure of a loess in China

Zhen Liu, Fengyin Liu, Fuli Ma, Mei Wang, Xiaohong Bai, Yonglai Zheng, Hang Yin, and Guoping Zhang

Z. Liu and H. Yin. Department of Civil and Environmental Engineering, Louisiana State University, Baton Rouge, LA 70803, USA

F. Liu. School of Civil Engineering and Architecture, Xi'an University of Technology, Xi'an, Shaanxi, 710048, China

F. Ma, M. Wang, and X. Bai. College of Architecture and Civil Engineering, Taiyuan University of Technology, Taiyuan, Shanxi, 030024, China

Y. Zheng. Department of Hydraulic Engineering, Tongji University, Shanghai, 200092, China

G. Zhang. Department of Civil & Environmental Engineering, University of Massachusetts Amherst, Amherst, MA 01003, USA

Corresponding author: Guoping Zhang (e-mail: zhangg@umass.edu).

Abstract

The collapse potential, mineralogy, microstructure, and particle morphology of a loess from the Loess Plateau, China, were characterized by double oedometer testing, X-ray diffraction, scanning electron microscopy with energy-dispersive X-ray spectroscopy, and image analysis to elucidate the origin of its collapse behavior. Results show that the loess is highly collapsible with a maximum collapse index of 6.7% at a vertical stress of ~200 kPa. The deposit contains both non-clay (i.e., quartz, albite, muscovite, and calcite) and clay (i.e., two chlorites) minerals. Microstructural, chemical, and image analyses indicate that interparticle calcite and clay cementation and silt particle morphology render the intact soil a metastable structure. Wetting-induced collapse is attributed to both primary and secondary microstructure features. The former is the abundance of weakly cemented, unsaturated, porous pure clay and clay-silt mixture aggregates whose slaking upon wetting initiates the overall structural collapse, while the latter consists of high porosity, unstable particle contacts, and clay coating on silt particles that act synergistically to augment the collapse. A conceptual microstructural model of a four-tiered hierarchy (i.e., primary clay and silt particles, clay aggregates and clay-coated silt particles, clay-silt mixture aggregates, and cemented aggregate matrix) is proposed to represent its structural characteristics and to account for its high collapsibility.

Key words: Collapsibility, Loess, Microstructure, Mineralogy, Particle morphology, Silt

Introduction

Loess, an aeolian, non-stratified deposit, is composed of primarily silt-sized particles with small fractions of clay and sand particles. It occurs widely around the world, including Asia, Africa, central and southern Europe, Antarctica, northwestern and central USA, northern Russia, interior Alaska, and South America (e.g., Argentina), among others (e.g., Porter 2007; Roberts et al. 2007; Rousseau et al. 2007; Zárate 2007). Of these regions, China has the most extensive distribution of loess including layers with the greatest thickness (Sun 2002). The Loess Plateau in northern and northwestern China with an arid to semi-arid climate occupies a total area of about 65×10^4 km^2 (i.e., more than 6% of the territory of China) (Tan 1988; Miao and Wang 1990). Because of its collapse behavior and other associated geotechnical engineering issues, such as wetting-induced landslides, hydroconsolidation, and seismic settlement, loess belongs to problematic soils and has been the subject of geotechnical research and practice since the 1960s (Feda 1988; Dijkstra et al. 1994; Rogers et al. 1994; Dijkstra et al. 1995; Derbyshire 2001; Delage et al. 2005; Xu et al. 2007; Yuan and Wang 2009).

Loess is a particulate earth material and, just like other geomaterials, its behavior and engineering properties are dominantly and sometimes solely controlled by its mineralogical composition and structure, including macroscopic texture and microstructure. The mineral particles of a soil make up the essential solid skeleton for load bearing and force transmission. Furthermore, mineralogy also affects the mechanical behavior (e.g., particle crushing strength, hardness or local yielding, elasticity, and interparticle friction) of individual particles and is the primary factor controlling their morphological properties (e.g., size, shape, and surface texture) (Mitchell and Soga 2005). Soil structure refers to both fabric and the non-frictional interparticle forces between adjacent soil particles (Lambe and Whitman 1969). The former is usually defined

as the arrangement and association of particles, particle groups, and pore spaces. Soil structure dominantly affects its mechanical and hydromechanical properties (da Silva and Kay 2004; Zhang et al. 2004; Lin et al. 2005; Mitchell and Soga 2005; Kay et al. 2006; Monroy et al. 2010). In fact, Oda (1972) pointed out that a detailed study of the morphological and physical properties of a soil's granular particles and their configurations (i.e., fabric) should be performed before its mechanical properties can be elucidated.

The importance of soil structure to the understanding of loess collapse behavior and other loess-related geohazards is demonstrated by some recent efforts. Miao and Wang (1990) proposed a hypothesis that loess collapsibility is caused by certain instability in its microstructure. Assallay et al. (1997) investigated the formation of open structure in a loess and pertinent collapse using laboratory-prepared specimens, and concluded that the nature of loess particles and microstructure play an important role in its structural collapse. They further stated that particle size, one of the structural parameters, is also a key control for structural collapse and other related effects. Tu et al. (2009) developed a method to analyze slope failure in loess based on a full-scale field experiment and attributed the rainfall-induced landslides to structural collapse. Yuan and Wang (2009) attempted to link the collapsibility with seismic settlement in a loess, and concluded that both the collapsibility and seismic settlement are correlated to its metastable microstructure, but with different triggering mechanisms. Giménez et al. (2012) characterized a loess in central Spain with a special perspective in microstructure analysis. It was further noted by Rogers et al. (1994) that a change in particle packing is central to loess collapse. Deng et al. (2007) analyzed a series of microstructural images of loess samples from six different sites and found that the trellis pore areas and particle size distributions are well correlated with the seismic subsidence coefficient. However, despite these efforts, current understanding of the

underlying mechanisms controlling loess collapse behavior and the origin of collapsibility still remains controversial or incomplete.

This paper presents an extensive study that aimed to further probe the fundamental mechanisms of loess collapsibility based on particle-level characterization (e.g., microstructure, composition, cementation, and particle morphology) and hence elucidate the origin of collapsibility using a loess from the Loess Plateau in northwestern China. A systematic experimental program was developed to characterize the soil's collapsibility, mineralogy, microstructure, cementing agents, and silt particle morphology. It is expected that the results from these characterization can lead to an in-depth understanding of the collapse behavior, particularly the trigger of collapse upon wetting and subsequent evolution of the microstructure.

Materials and methods

Samples

Undisturbed block samples of typically 20 × 20 × 20 cm were collected at a depth of 5.0 m below the ground surface from an open excavation pit in Xi'an, which is located within the major occurrence of the Loess Plateau in China (Figure 1a). Immediately after retrieval from the ground, samples were carefully wrapped in situ by multiple layers of plastic film, aluminum foil, and duct tape to minimize water content change and sample disturbance. Particular care was also taken during transportation to and storage in the laboratory to keep disturbance and waster loss as minimal as possible.

The soil profile at the sampling site is shown in Figure 1b. The loess in China is subdivided into three major stratigraphic units, from the youngest to the oldest: Malan (Q_4^{ml}), Lishi (Q_3^{1eol} and Q_3^{2eol}), and Wucheng (Q_2^{eol}) loess (Dijkstra 2001). The groundwater table is at a

depth of 12.0 m. The samples thus belong to the Lishi (Q_3^{1eol}) loess and are unsaturated. Some basic physical and index properties of this loess obtained via relevant ASTM standard test methods (ASTM 2009) are summarized in Table 1. Particle size analysis through combined wet sieving and hydrometer shows that the sample consists of dominantly silt particles with a fraction of 77.0% and secondarily clay particles with a fraction of 19.4%. With a sand fraction of 3.6% that can be essentially ignored, the loess is made of mostly clay and silt particles. Its median particle size (D_{50}) is 12.0 μm, confirming that silts are the dominant particles. Its in-situ density of 1.52 Mg/m^3 further suggests that the sample belongs to the Lishi that has bulk densities ranging from 1.7 (base) to 1.4 (top) Mg/m^3 (Dijkstra 2001). Figure 2 shows the classification of different loesses proposed by Gibbs and Holland (1960). According to this chart, the studied loess belongs to the category of "silty loess". Despite its dominant silt fraction, it is a low-plasticity clay (CL) with a liquid limit of 30.0% and a plastic index of 10.7%, according to the Unified Soil Classification System (USCS) (Table 2). Such a classification agrees well with prior findings that most loesses usually have a low plasticity index (Delage et al. 2005).

Collapsibility measurement

To assess the collapsibility of the loess sample, the widely used "double oedometer" method was employed (Jennings and Knight 1957; Clemence and Finbarr 1981). Two oedometer specimens were trimmed from the intact block samples. The first one was loaded at its natural water content during the entire test, while the other was inundated at a vertical stress of 50 kPa. Based on their compression curves, the collapse index (I_c) is defined as (ASTM 2009):

$$I_c = \frac{H_p - H'_p}{H_0} \times 100 \quad (1)$$

where H_p and H_p' are the stabilized heights (i.e., the heights at the end of a load increment) of specimens at the natural and "inundated" water contents under a given vertical stress p, respectively, while H_0 is the initial height of the specimen. Incremental loading with vertical stresses ranging from 25 to 1200 kPa was employed in the double oedometer tests. To better define the compression curves and yielding points, the adopted load increment ratio (i.e., the ratio of the change in effective stress between two consecutive loadings to the effective stress of the former loading, $\Delta\sigma_v' / \sigma_v'$) was smaller than 1.0. For each load increment, the load remained constant for 24 hours or until no further deformation occurred, particularly for the specimen tested at its natural water content.

Mineralogical analysis

X-ray diffraction (XRD) was performed to characterize the mineralogy of the loess sample. Totally four different samples were analyzed to positively identify its mineralogy. Since wetting causes its structural collapse and strength loss, an undisturbed sample block was first inundated with deionized water to introduce collapse, followed by air-drying. Such a sample having undergone a cycle of pre-wetting and air-drying was hence termed "disturbed". The reason for studying such a "disturbed" sample is to examine whether highly soluble minerals are present or whether wetting-drying can alter the mineralogical composition of the soil. The disturbed sample was then gently crushed and dry-ground by hand in a mortar with a pestle until all particles passed through a No. 340 sieve (i.e., a mesh opening size of 44 μm) (which required excessive grinding), resulting in the first powdery sample (i.e., "disturbed – dry ground") for XRD analysis. Because intensive or high-energy dry-grinding tends to cause structural or chemical changes to certain minerals (e.g., clays), the disturbed sample was also wet-ground for

3 minutes with ethyl alcohol in a McCrone micronizing mill (McCrone Accessories and Components, USA), resulting in the second powdery sample (i.e., "disturbed – wet ground"). The third sample was prepared by the same procedures used to prepare the second one, except that the initial sample was not subjected to pre-wetting with deionized water, but was air-dried slowly from the intact state. Thus it is termed "undisturbed – wet ground". The fourth one, termed "clay fraction only", was the clay (i.e., <2 μm) fraction extracted from the loess sample via sedimentation (e.g., Moore and Reynolds 1997). A side-loading method was used to mount sample powder into an aluminum sample holder to reduce preferred orientation of the clay particles. XRD patterns were obtained in a Bruker/Siemens D5000 automated diffractometer using Cu *K*α radiation with an excitation energy of 40 kV and 30 mA, a step size of 0.02°, a scan speed of 0.02° per 2 seconds, and diffraction angles (2θ) of 2 to 42°. The peaks in the diffraction patterns were analyzed and identified by the Jade 9.3.3 Program (Material Data, Inc.).

Microstructural characterization

One intact sample block was carefully selected for microstructural characterization. First, two small cuboids with the same dimension of 30 × 30 × 15 mm (length × width × thickness) were trimmed out of the central part of the selected block, with the orientation clearly marked as "V" and "H" for vertical and horizontal surfaces, respectively, followed by air-drying in laboratory ambient environment (e.g., Dathe et al. 2001). Because their size was small, the shrinkage was expectedly insignificant. After air-drying, the changes in the three dimensions were all less than 1.0%, indicating that drying-induced shrinkage or disturbance was not a major concern. Because of its susceptibility to collapse upon wetting, these traditional liquid-based porewater removal methods that are developed for saturated soft clays were not employed. In

fact, preliminary trials showed that the intact loess collapsed upon submersion in alcohol or acetone.

Sample impregnation used a mixture solution containing epoxy resin, acetone, ethanediamine, and dibutyl phthalate at a volume ratio of 100 : 200 : 7 : 2. The air-dried soil cuboids were first placed inside a clean aluminum cup with its bottom covered by a thin layer of clean coarse sand to facilitate subsequent uniform seepage of the solution into the sample. Impregnation took place in a sealed desiccator holding the cup together with the soil cuboid. A high vacuum pressure of 0.02 MPa was first applied to de-air the sample, followed by extremely slowly dripping the impregnation mixture solution into the cup. With continuous dripping, the surface of the solution moved up very slowly inside the cup. This process was stopped when the soil cuboid inside the cup became fully submerged to a depth of >10 mm. Then the soil cuboid was allowed to harden slowly inside the cup for ~3 months, followed by cutting into thin sections of 12 × 14 × 4 mm (Wang et al. 2010). Both horizontally and vertically cut thin sections denoted hereafter as “Sample H” and “Sample V”, respectively, were obtained.

Microstructural characterization was performed on these thin sections using an FEI Quanta 200 3D FEG scanning electron microscope (SEM). Before SEM scanning, the surfaces of the thin sections were sputter-coated with platinum (Pt). Chemical elemental analyses were also performed by a built-in energy-dispersive X-ray spectroscopy (EDXS) detector on selected areas or spots of interest. Particular attention was paid on the elemental composition of some individual soil particles (e.g., silt particles) and the cementing agents among particle contacts.

Image analyses

Image analyses were conducted on a selected SEM micrograph to quantify particle morphology, particularly particle size and shape. Because of aggregation and attachment to other particles, individual clay particles could not be isolated and identified under regular SEM magnifications. In addition, clay particles and small silt particles mainly serve as the cohesive material in the microstructure of loess (Gao 2011). Therefore, particle size and shape analyses focused on relatively large silt particles with a size of >5 μm. An SEM image containing plenty of silt particles was carefully selected, and individual silt particles with clear boundaries were isolated manually, resulting in a black-and-white image with the black color representing particles. Then the particle morphology was analyzed by an image analysis program, ExpertShape (V4.09). Because a great number of silt particles with varying shapes and sizes were considered, the particle morphology parameters obtained from ExpertShape were further statistically analyzed.

Form (overall shape), roundness (large-scale smoothness), and surface texture (small-scale smoothness) are three independent properties describing particle shape (Barrett 1980). In this study, characterization of surface texture and roundness was not feasible, owing to the relatively small size of silt particles and the low magnification used in the selected SEM image. Therefore, four different particle morphology properties were quantified for the silt particles in the selected SEM image, including sphericity, elongation, circularity, and equivalent circular diameter (ECD), of which the former three describe some form aspects of particle shape, while the last one is related to particle size. It should be noted that these shape properties were obtained from a two-dimensional SEM image and their definitions were also based on two-dimensional measurements.

Sphericity is defined as the ratio of radius of the inscribing circle to that of the circumscribing circle. The inscribing and circumscribing circle radii are the shortest and longest distances from the contour of the particle to its gravity center, respectively. Elongation is defined as the difference between 1.0 and the aspect ratio, which is the ratio of the minimum Feret diameter to the maximum Feret diameter. The maximum and minimum Feret diameters are the longest and shortest distances between two parallel tangents touching opposite sides of a particle. The high sensitivity (HS) circularity (f_{circ}), depending on both the form and roundness, is used to describe the compactness of a particle (e.g., a circle is the most compact shape). It is defined as the ratio of the area of the particle in its original shape to the area of a circle having the same perimeter of the particle. For instance, f_{circ} is 1, $\pi/4$, and 0 for a circle, a square, and an infinitely long and narrow shape, respectively. The value of f_{circ} ranges from 0 to 1. Finally, because of the difficulty in providing one single dimension to represent the size of an irregularly shaped particle, the ECD is also selected to quantify silt particle size via image analysis. It is the diameter of an equivalent circle having the same area (A) as the original particle:

$$ECD = 2\sqrt{\frac{A}{\pi}} \tag{2}$$

Analyses of results

Collapse index

Figure 3 shows the results from the double oedometer tests. The compression curves indicate that the soil at its natural water content and intact structure has a yield stress of ~100 kPa, slightly greater than the in-situ overburden pressure of 74.5 kPa (see Table 1 for in situ density). This indicates that the loess is slightly overconsolidated, most likely due to surface erosion-related unloading, presence of interparticle cementation (including clay and calcite cementations),

and particle morphology (e.g., angularity and sphericity) (Pestana and Whittle 1995), some of which will be discussed later. The compression curve of the specimen inundated at 50 kPa shows no apparent yielding-related curvature in the stress range of 50-1200 kPa, indicating that structural collapse may start at stresses of even <50 kPa.

The collapse index increases at low stresses (i.e., 50-300 kPa) and then decreases rapidly beyond 300 kPa. The maximum collapse index of this loess is 6.7%. According to the ASTM standard (ASTM 2009), this loess has moderately severe collapsibility. To elucidate the origin of its collapsibility, the soil composition, microstructure, and particle morphology were further characterized using a variety of techniques, and results are presented hereafter.

Soil mineralogy

Figure 4 shows the XRD patterns of the four processed loess samples. For the "disturbed – dry ground" sample, there are no peaks in the range of 2-20° 2θ, while the peaks in the range of 20-42° 2θ indicate the presence of non-clay minerals, including quartz (SiO_2), albite (a plagioclase feldspar, $NaAlSi_3O_8$), and calcite ($CaCO_3$). For the "disturbed – wet ground" and "undisturbed – wet ground" samples, their XRD patterns are nearly identical, indicating that simple wetting with deionized water does not cause detectable change in mineralogical composition. In addition to the above three non-clay minerals, two phyllosilicates, nimite and muscovite, are identified. The former is a chlorite, while the latter is a mica. Dry grinding, particularly high-energy or excessive grinding, can reportedly cause the deterioration and collapse of the crystalline structure of fine-grained clay minerals (Garcia et al. 1991; Kristof et al. 1993). Thus, the absence of clay minerals in the smaller diffraction angles of the "disturbed – dry ground" sample is believed to be caused by excessive dry grinding, which damaged the crystal

structure of phyllosilicates (e.g., muscovite, nimite). Such a collapse of crystal structure usually results in the clay minerals being amorphous to XRD.

The XRD pattern of the "clay fraction only" sample shows the presence of both muscovite and clinochlore, the latter being a chlorite. Noteworthy is that the extraction of clay fraction results in a much higher concentration of clinochlore in the clay fraction that may be otherwise too low in the bulk sample to be detectable by XRD. In fact, the absence of clinochlore in the other three patterns suggests that this chlorite is mainly present in the <2 μm fraction, while the other chlorite, nimite, mainly exists in the >2 μm fraction. Moreover, the pattern of the fourth sample also suggests that some fine quartz and calcite be present in the clay fraction. In this pattern, the broad peaks of clinochlore and muscovite, when compared with those peaks of muscovite and nimite from the third sample, imply that the muscovite and clinochlore in the <2 μm fraction are not as well crystalized as those in the bulk sample.

Regarding their origins, quartz and albite are most likely inherited from the initial wind deposition. Calcite can be both primary and secondary. The primary one is inherited from initial wind deposition and usually is present as solid mineral particles, while the secondary one is post-depositionally formed or reprecipitated in-situ and is usually believed to be a cementing agent. Two hypotheses can be used to explain the formation of calcite cementation: (1) groundwater (even at a great depth) that contains dissolved Ca^{2+} may move upward due to excessive drying and evaporating from the ground surface, and after water evaporates Ca^{2+} can react with atmospheric CO_2, resulting in the reprecipitation of $CaCO_3$ on particle surfaces and between particle contacts (Righi and Meunier 1995); and (2) weathering of the primary calcite and dolomite minerals results in the leaching of Ca^{2+} to the groundwater, which can then react with atmospheric CO_2 to precipitate as calcareous cementation. This synergetic process is also called

"loessification" (Derbyshire et al. 1998; Derbyshire 2001; Delage et al. 2005). The newly formed calcite can then act as a cementing mineral that exists on the surfaces of other particles as coating or between particle contacts as bridging. These formations can then lead to an increase in soil's stiffness and strength. This is possibly one mechanism contributing to the "apparent overconsolidation" of the intact loess.

According to the literature, another mechanism responsible for the "apparent overconsolidation" of usually unsaturated in situ loess is clay cementation whose identification will be discussed later. For this specific loess, clinochlore and nimite are the identified clay minerals present in the soil. At its natural water content of 20.3%, the net negative surface charges of clay minerals can induce electrostatic interactions with other mineral particles. Together with van der Waals forces, the electrostatic interactions can act as bonding holding clay particles and other silt particles together. Thus, the in-situ intact soil can gain further enhancement in yielding and stiffness via clay cementation, in addition to calcite cementation.

In summary, the loess sample contains quartz, albite, muscovite, and calcite as the non-clay minerals, and two chlorites, nimite and clinochlore, as the clay minerals (Table 2). It is noteworthy that iron oxides were not identified from these XRD patterns, despite the soil exhibiting a light brown and yellowish color. This may be caused by two possible reasons: (1) their concentrations are too low to be detected by XRD, and (2) the iron oxides (that may include hematite or goethite) are amorphous. A definitive identification and quantification warrants further investigation. However, prior studies concluded that two widely occurring iron oxides, hematite and goethite, are present in loess in China (Jiang et al. 2012). In fact, it is the iron oxides that render the loess a yellowish to brownish color (Schwertmann and Taylor 1989; Zhang et al. 2004).

Microstructure

The microstructural characterization discussed in this section is mainly observational and qualitative in nature. The focus is on the particle association and arrangement, porosity, and interparticle contacts. Quantitative analysis of particle morphology (i.e., shape and size) is presented in next section.

Overview of microstructure: Figure 5 compares four selected SEM images showing the overview of the loess microstructure. First of all, angular or subangular silt particles that can be clearly identified by their size and solid texture are randomly oriented and distributed, and the interparticle zones are either voids or filled by much smaller clay particles. Occasionally, a silt particle shows chipped edges or impact cracks. Although it has been reported that most loesses are homogeneous (Delage et al. 2005), the studied one shows certain heterogeneity at the smaller scale. Some areas are densely packed, while others are very porous. Clearly, bedding planes are absent in both the horizontal and vertical surfaces. The lack of bedding and a random orientation and distribution of different sized particles together with their subangular and angular shapes are characteristic to the nature of this soil's aeolian deposition.

Particle association: A careful examination of the images in Figures 5c and 5d and Figure 6 can find that the clay and silt particles are typically associated together to form aggregates. The size of aggregates varies significantly, ranging from tens to hundreds of micrometers. In fact, aggregates with a size of 100-300 μm can be identified in Figure 5c. While most aggregates consist of both silt and clay particles, some are made up of purely clay particles (Figure 7a). Moreover, it appears that the surface of most silt particles is covered by a thin layer of coating (as indicated by the white external boundary on these particles), which could be secondary

carbonates (BeczeDeak et al. 1997) or amorphous silica (Delage et al. 2005). In addition, clay particles can also act as coatings over silt particles (Clemence and Finbarr 1981), which is a distinct association promoting the connection of silt particles by clay cementation. Some clay aggregates are also mixed with or sandwiched by muscovite particles.

Porosity: Pores with a wide variety of sizes can be observed in Figure 6 (note that the dark zones are the pore space). Large pores of >150-200 μm can be clearly observed in Figures 5a and 5b, while smaller ones of a few to tens of micrometers are shown in Figures 5c and 5d. In general, large pores are formed between aggregates, while smaller ones exist within aggregates.

Particle contact: Another important microstructural feature is particle contact, which controls the onset of relative movement between particles. Two distinct features should be pointed out here: (1) a metastable structure formed by a thin chain of relatively small silt and clay particles (Figures 5b and 5d); and (2) unstable points or contacts, which are an important aspect of initial microstructure formation because they could collapse more easily and contribute to the structural breakdown or evolution (Assallay et al. 1997). Figure 7a shows the unstable point, while a higher resolution with more details is shown in Figure 7b. With a small disturbance or the collapse of the pure clay aggregate beneath Particle P1, the contact point of the three silt particles, P1, P2, and P3, becomes unstable, leading to localized collapse that may trigger further structural collapse.

Cementation: It is well known that loess usually contains both calcite and clay cementations to support its stability at its unsaturated state. While direct observation of calcite cementation is difficult due to its very small dimension or special morphology as coatings or bridging, clay cementation is clearly observable (Figure 6). In general, silt particles are randomly and loosely distributed, and bridged to each other by clay-based connectors (i.e., clay

cementation). On some occasions, clay coating on silt particles and clay cementation are not differentiable (e.g., the curved chain of clay and smaller silt particles, Figure 5b). The presence of calcite is identified by XRD, and the possible mechanisms for the formation of calcite cementation are also discussed previously. Therefore, both calcite and clay cementations act as bridging and bonding between silt particles.

Particle morphology

Figure 8a shows the SEM image selected for silt particle morphology analysis, because it contains a large amount of silt particles but much less pores. Figure 8b shows the pertinent image where all silt particles of ≥5 μm in size were individually identified and isolated, but clays and pores were excluded. It should be noted that the particles touching the border were removed to avoid treating parts of a particle as a whole one. A total of 197 silt particles were identified and analyzed. Clearly, these particles are mainly angular to subangular in roundness according to the classification chart developed by Mitchell and Soga (2005), and some are even lanky with a large aspect ratio (e.g., the ratio of length to width). Given that the overall void ratio is e_0 = 1.19 (Table 1), the total areas of all silt particles and of all clay particles in Figure 8b are estimated to be 33,880 and 48,523 μm^2. Thus, the ratio of the area occupied by silt to that by clay is estimated to be 0.69, indicating that the silt particles only occupy about two-thirds of the area occupied by clay particles. It also implies that the deformation of the entire loading-bearing skeleton of this loess is controlled by clay fraction, although its weight fraction is only 19.4% and the silt's weight fraction is 77.0%. Such a phenomenon may suggest that the collapsibility be mainly controlled by the clay particles and their associations (e.g., clay aggregates, clay coating on silt particles, and clay cementation).

Figure 9 summarizes the statistical results of particle shape parameters (i.e., sphericity, HS circularity, and elongation) together with the size parameter (i.e., ECD) in terms of probability density function (PDF) and cumulative distribution function (CDF) curves. The ECD follows a lognormal distribution, while the other three shape parameters obey arithmetic normal distributions. In fact, most particle size distributions (PSDs) exhibit a lognormal distribution. In a critical review, Barrett (1980) also concluded that most shape parameters of rock particles have arithmetic normal distributions.

As shown in Figure 9a, the ECD ranges from 5 to 44 μm with a median of 13.6 μm, demonstrating that all isolated particles in Figure 8b are indeed silt particles (i.e., a size range of 2 to 75 μm), consistent with other work (e.g., Sun et al. 2006). The PSD CDF curve (i.e., the plot of percent finer by weight vs. particle size for silt particles only) obtained by the ASTM standard method (Table 1) is also plotted in Figure 9a, with a coefficient of curvature C_c = 0.93 and a coefficient of uniformity C_u = 4.21. If the Unified Soil Classification System (USCS) criteria developed for the sand gradation are valid for silts, then the silt particles in this loess are poorly graded. Similarly, another parameter, a sorting coefficient (S_0), defined as the square root of the ratio of the larger quartile to the smaller quartile, is also used to define the degree of sorting (i.e., a measure of the spread of PSD). The silt particles shown in Figure 8b have an $S_0 = 1.32 < 2.5$, indicating that they are well sorted (Trask 1932). Therefore, the two criteria used to determine the gradation of silt particles yield consistent results. Moreover, the well sorting of silt particles also supports the nature of aeolian deposition of this loess.

Regarding the shape of silt particles, the HS circularity has a mean value of 0.71, showing that they are more close to a square (which has an HS circularity of π/4), in terms of form and roundness. The value of elongation ranges from 0 to 1. For instance, a particle with a

shape symmetrical in all axes (e.g., a square or circle) has an elongation of 0, and a particle for which the difference between the minimum and maximum Feret diameters is large yields an elongation value of ~1. For the silt particles, the mean value of elongation is 0.39, which is closer to the lower range (i.e., 0) than to the higher range (i.e., 1.0). To some extent, this also suggests that the silt particles are more close to a square, consistent to the results of HS circularity. A mean sphericity of 0.44 indicates that a considerable percentage of particles have a shape of concave polygon, although the overall form is close to a square. Such a particle geometry is most likely caused by the particle-to-particle collisions during transport by wind, which results in chipped or indented edges (Delage et al. 2005). In summary, quantitative particle shape analyses show that the silt particles are more of a square in terms of form and angular and subangular in terms of roundness. However, some particles have a shape of concave polygon resulting from particle collisions during aeolian transport.

EDXS elemental analysis

Figure 10 shows the spots of EDXS chemical analysis performed on two different zones selected from the Samples V and H, and corresponding results are summarized in Table 3. Figure 11 shows some selected EDXS spectra to demonstrate the elemental compositions of spots of interest.

From Figure 11, Spot 1 in Sample V and Spot H4 in Sample H only contain C, O, and Cl. These two spots are the dark zones or voids filled with epoxy resin ($C_{21}H_{25}ClO_5$), one of the major chemicals used for sample impregnation. Because of its very low atomic weight, H in the clay minerals and epoxy resin cannot be detected by EDXS (Garratt-Reed and Bell 2005). Therefore, the dark zones are epoxy resin. Spot 2 in Sample V is a particle and its EDXS

spectrum shows the presence of C, O, and Ca, indicating that it may be a primary calcite; the trace Mg indicates some substitutions of Ca by Mg in the calcite. Spot 18 has a complex spectrum that shows the presence of C, O, Mg, Al, Si, K, Ca, and Fe, suggesting that it may be clay minerals with calcite cementation. Finally Spots 17 and 7 may be an albite ($NaAlSi_3O_8$) with calcite coating and quartz, respectively. Similarly, for Sample H (Figure 11b), Spots H5 and H6 can be an albite and quartz particle, respectively.

As shown in Table 2, C, O, Mg, Ca, Na, Al, Si, K, Ni, F, and Fe from the EDXS analysis match well with the composition of those minerals identified by the XRD, including chlorites, muscovite, quartz, albite, and calcite. Cr has been found to exist in clinochlore (Phillips et al. 1980); Ti has also been detected in clinochlore and nimite (Phillips et al. 1980; Zhan and Guggenheim 1995). For the bright spots that are the external boundary of particles (it should be noted that not all particle boundaries are shown as bright spots), the elements detected by EDXS suggest that there are clay minerals acting as coating on the surfaces of silt particles. That is why there exist more chemical elements (e.g., Na, Mg, Al, and K) as well as Si and O for the particles, strip-like particles, and tips of particles (Spot 17) in Sample V. The elements in the interparticle zones are identified as Si, Ca, Fe, O, and Al, which are the main chemical elements of clay minerals. Together with the result of the bright spots, it can be concluded that the filling material between silt particles are clay minerals. The result from an aggregate-like spot (Spot 5 in Sample V) supports this statement.

Discussion

A conceptual microstructure model

A comprehensive synthesis of the above results on the mineralogy, elemental composition, microscopy observations, and particle morphology provides a clear understanding of the microstructure. Based on the developed understanding, a conceptual microstructure model of a four-tiered hierarchy with increasing length scale and complexity is proposed to delineate the particle-level interactions and associations within a representative volume element (RVE) (Figure 12). The proposed microstructure model is established via a bottom-up (i.e., from smaller to larger length scales) approach to ease interpretation and understanding. At the smallest length scale, Tier I is the basic, primary <2 μm clay particles and 2-75 μm silt particles, the latter occurring occasionally as separate, functional units (e.g., load-bearing for structural stability). Here a silt particle with carbonate or silica coating is treated the same as a monolith particle. However, a majority of primary particles do not exist as individually functioning units, but form pure clay aggregates and clay-coated silts, which are the two major, relatively larger and complex units defined in Tier II (Figure 12). In Tier III, even larger clay-silt mixture aggregates form, which may consist of pure clay aggregates, silt particles, and clay-coated silt particles as well as the clay and calcite cementations among these units. Tier IV deals with the overall representative structure for the RVE where all of the sub-units in Tiers I to III may all occur randomly. Noteworthy are the presence of relatively small intraaggregate pores in the pure clay aggregates and clay-silt mixture aggregates and the formation of relatively large interaggregate pores. Such porosity features render the soil a highly porous structure. Finally, calcite and clay cementations exist within individual aggregates and between adjacent aggregates, rendering the loess a relatively stiff and stable structure at its natural state. Such a structure model also takes

into account the mineralogical composition of the loess explicitly. The clay particles are mainly two chlorites, nimite and clinochlore, and the silt particles are quartz, albite, muscovite, and calcite (Table 2). Both clay minerals and secondary calcite can be the interparticle and interaggregate cementations.

Origin of collapsibility

The above conceptual microstructure model clearly demonstrates that the loess possesses a metastable or collapsible structure. In its natural, intact state (i.e., usually unsaturated), the high suction within the clay aggregates, clay and carbonate cementation, and the angularity of silt particles provide sufficient cohesion and friction, resulting in a metastable structure that renders the soil considerably high strength and stiffness at its intact state.

However, upon inundation or wetting, hydration of clay particles commences, resulting in the expansion of electrical double layers on their surfaces. It is well known that fully hydrated clays with expanded electrical double layers exhibit much smaller internal friction angle than clays with less hydration. Such a process of clay hydration is also usually accompanied by slaking of clay aggregates and clay cementation (i.e., detachment and separation of clay coating from silt particles) (Barden et al. 1973; Mitchell and Soga 2005), leading to the first step in structural collapse (i.e., slaking of clay aggregates and breakdown of clay cementations). Such an initial collapse may not be severe if the calcite cementation is not completely broken. With increasing loss of high suction stress (i.e., decrease in effective stress) and/or an increase in external loading, calcite cementation can then breakdown, resulting in further damage to the intact structure. The corresponding macroscopic phenomenon is the collapse of the entire structure, accompanied with large surface settlement (Figure 12).

In summary, the moderately severe collapsibility originates from both the compositional and microstructural characteristics of the loess. The former consists of a low water content (i.e., an unsaturated state) and a significant volume occupied by clay and clay associations (e.g., individual clay particles, clay coatings on silt particles, and clay cementation), while the latter includes mainly the presence of weakly cemented pure clay and clay-silt mixture aggregates and the high porosity (including relatively larger interaggregate pores and smaller intraaggregate pores), as well as calcite cementation (which also supports a metastable structure in its intact state).

Engineering implications

Because of the collapsibility, loess is regarded as one of the worst problematic soils that geotechnical engineers have to deal with in engineering practice. The elucidation of the loess microstructure and its mineralogical composition can help understand some peculiar engineering behavior and properties of loesses, and such an developed understanding can be exploited by engineers in the design and construction of buildings and facilities built on or in the loess deposits, as well as for future research activities.

The high suction associated with the natural unsaturated state (i.e., a low nature water content of 20.3% and degree of saturation of 46.1%), the presence of calcite and clay cementations, and the distinct morphology of dominant silt particles (i.e., the high angularity and high sphericity) provide a synergy for the apparent preconsolidation pressure exhibited by the natural, intact loess. However, caution must be taken when applying the results obtained from intact, unsaturated samples to situations where the loess can have free access to water. In addition, the moderately severe collapsibility of the loess originates from a combination of

several major structural features, including the presence of pure clay and clay-silt mixture aggregates, clay cementation, high porosity, and metastable and unstable particle contacts. However, the trigger is the hydration and wetting of clay aggregates and clay cementation, leading to the slaking, detachment, and breakdown of clay aggregates, clay coating, and clay cementation, respectively. Only does after this first step of collapse occur, progressive failure followed by structural avalanche takes place to augment the collapsibility. In fact, such a characteristics has not been so well documented in the literature.

The above conceptual microstructure model of a four-tier hierarchy also suggests some peculiar features for the loess microstructure. First of all, although the loess consists of exclusively clay and silt particles (i.e., Tier I), they usually are not present as separate, individually functioning units. Instead, they form larger aggregates of varied composition and length scales (i.e., Tiers II and III). Such a hierarchical structure also indicates high porosity, and its metastable fabric with interparticle cementation implies high compressibility upon structural collapse. Such a better delineation of the loess microstructure may provide a detailed basis for the formulation of constitutive soil models as well as the modeling of soil behavior under different loading conditions using prevailing numerical analysis techniques, such as finite element and discrete element methods (Jiang et al. 2012).

Conclusions

A series of laboratory characterization was performed to determine the collapse potential, mineralogy, microstructure, and silt particle morphology of a loess in Xi'an, China, to identify and elucidate the origin of its collapsibility. The integration of experimental results, observations, and analyses leads to the following major conclusions:

- The loess exhibits a moderately severe collapse potential, as indicated by its maximum collapse index of 6.7% at a vertical stress of ~200 kPa.
- The soil consists of two chlorites, nimite and clinochlore, as the major clay minerals and muscovite, quartz, albite, and calcite as the non-clay phases. Both primary and secondary phases of calcite may be present in the soil, and the latter is likely the major cementing agent. Other non-clay minerals (except muscovite) are present as silt particles of angular and subangular in roundness.
- While occasionally a clean silt particle is present, the majority of silt particles are covered with clay coating and/or associated with clay particles to form hybrid silt-clay mixture aggregates. In addition to calcite cementation, clay particles also act as bridging (i.e., clay cementation) between silt particles and clay aggregates.
- Regarding the morphology of silt particles, the mean values of the ECD, HS circularity, sphericity, and elongation are 13.56 μm, 0.71, 0.44, and 0.39, respectively. These data indicate that the silt particles are more close to a square in the view of form and are well sorted.
- The proposed conceptual microstructure model of a four-tiered hierarchy with increasing length scale and complexity can be used to delineate the particle-level associations and interactions and to elucidate the origin of collapsibility.

Acknowledgments

This study was partially supported by the National Natural Science Foundation of China (Award Nos. 50478096 and 51128901). Zhen Liu is partially supported by the Louisiana Board

of Regents EDA Award. Fengyin Liu was also partially supported by an NSF EPSCoR grant from Louisiana Board of Regents and National Science Foundation.

References

Assallay, A.M., Rogers, C.D.F. and Smalley, I.J. 1997. Formation and collapse of metastable particle packings and open structures in loess deposits. Engineering Geology, **48**, 101-115, doi: 10.1016/s0013-7952(97)81916-3.

ASTM. 2009. Annual Books of ASTM Standards. ASTM International, West Conshohocken, PA.

Barden, L., McGown, A. and Collins, K. 1973. Collapse mechanism in partly saturated soil. Engineering Geology, **7**, 49-60, doi: 10.1016/0013-7952(73)90006-9.

Barrett, P.J. 1980. The shape of rock particles, a critical review. Sedimentology, **27**, 291-303, doi: 10.1111/j.1365-3091.1980.tb01179.x.

BeczeDeak, J., Langohr, R. and Verrecchia, E.P. 1997. Small scale secondary CaCO3 accumulations in selected sections of the European loess belt. Morphological forms and potential for paleoenvironmental reconstruction. Geoderma, **76**, 221-252, doi: 10.1016/s0016-7061(96)00106-1.

Clemence, S.P. and Finbarr, A.O. 1981. Design considerations for collapsible soils. Journal of the Geotechnical Engineering Division-Asce, **107**, 305-317.

da Silva, A.P. and Kay, B.D. 2004. Linking process capability analysis and least limiting water range for assessing soil physical quality. Soil & Tillage Research, **79**, 167-174, doi: 10.1016/j.still.2004.07.005.

Dathe, A., Eins, S., Niemeyer, J. and Gerold, G. 2001. The surface fractal dimension of the soil-pore interface as measured by image analysis. Geoderma, **103**, 203-229, doi: 10.1016/s0016-7061(01)00077-5.

Delage, P., Cui, Y.J. and Antoine, P. 2005. Geotechnical problems related with loess deposits in Northern France. *Proceedings of International Conference on Problematic Soils*. Eastern Mediterranean University Press, Famagusta, North Cyprus, 517-540.

Deng, J., Wang, L.-M. and Zhang, Z.-Z. 2007. Microstructure characteristics and seimic subsidens of loess. Chinese Journal of Geotechnical Enginerring, 542-548.

Derbyshire, E. 2001. Geological hazards in loess terrain, with particular reference to the loess regions of China. Earth-Science Reviews, **54**, 231-260, doi: 10.1016/s0012-8252(01)00050-2.

Derbyshire, E., Meng, X.M. and Kemp, R.A. 1998. Provenance, transport and characteristics of modern aeolian dust in western Gansu Province, China, and interpretation of the Quaternary loess record. Journal of Arid Environments, **39**, 497-516, doi: 10.1006/jare.1997.0369.

Dijkstra, T.A. 2001. Geotechnical thresholds in the Lanzhou loess of China. Quaternary International, **76-7**, 21-28, doi: 10.1016/s1040-6182(00)00086-0.

Dijkstra, T.A., Rogers, C.D.F., Smalley, I.J., Derbyshire, E., Li, Y.J. and Meng, X.M. 1994. The loess of north-central China: Geotechnical properties and their relation to slope stability. Engineering Geology, **36**, 153-171, doi: 10.1016/0013-7952(94)90001-9.

Dijkstra, T.A., Smalley, I.J. and Rogers, C.D.F. 1995. Particle packing in loess deposits and the problem of structure collapse and hydroconsolidation. Engineering Geology, **40**, 49-64, doi: 10.1016/0013-7952(95)00022-4.

Feda, J. 1988. Collapse of loess upon wetting. Engineering Geology, **25**, 263-269, doi: 10.1016/0013-7952(88)90031-2.

Gao, L. 2011. *Study on microstructural effects on collapsibility of loess and its evaluation methods.* Ph.D., Dalian University of Technology, China.

Garcia, F.G., Abrio, M.T.R. and Rodriguez, M.G. 1991. Effects of dry grinding on two kaolins of different degrees of crystallinity. Clay Minerals, **26**, 549-565.

Garratt-Reed, A.J. and Bell, D.C. 2005. Energy-Dispersive X-Ray Analysis in the Electron Microscope. BIOS Scientific Publishers Limited.

Gibbs, H.J. and Holland, W.Y. 1960. Petrographic and Engineering Properties of Loess. *In*: US Department of the Interior, B.o.R. (ed.), Denver, Colorado.

Giménez, R.G., de la Villa, R.V. and Martin, J.A.G. 2012. Characterization of loess in central Spain: a microstructural study. Environmental Earth Sciences, **65**, 2125-2137, doi: 10.1007/s12665-011-1193-7.

Jennings, J.E. and Knight, K. 1957. The additional settlement of foundations due to collapse of sandy soils on wetting. *Proceedings of the Fourth International Conference on Soil Mechanics and Foundation Engineering*, 316-319.

Jiang, M.J., Hu, H.J. and Liu, F. 2012. Summary of collapsible behaviour of artificially structured loess in oedometer and triaxial wetting tests. Canadian Geotechnical Journal, **49**, 1147-1157, doi: 10.1139/t2012-075.

Kay, B.D., Hajabbasi, M.A., Ying, J. and Tollenaar, M. 2006. Optimum versus non-limiting water contents for root growth, biomass accumulation, gas exchange and the rate of development of maize (Zea mays L.). Soil & Tillage Research, **88**, 42-54, doi: 10.1016/j.still.2005.04.005.

Kristof, E., Juhasz, A.Z. and Vassanyi, I. 1993. The effect of mechanical treatment on the crysal structure and thermal behavior of kaolinite. Clays and Clay Minerals, **41**, 608-612, doi: 10.1346/ccmn.1993.0410511.

Lambe, T.W. and Whitman, R.V. 1969. Soil Mechanics. John Wiley & Sons, Inc.

Lin, H., Bouma, J., Wilding, L.P., Richardson, J.L., Kutilek, M. and Nielsen, D.R. 2005. Advances in hydropedology. *In*: Sparks, D.L. (ed.) *Advances in Agronomy, Vol 85*. Elsevier Academic Press Inc, San Diego, 1-89.

Miao, T. and Wang, Z. 1990. The Deformation Mechanism of Collapsible Loess based on Instability of Microstructure. Science in China,Ser.B, 86-96.

Mitchell, J.K. and Soga, K. 2005. Fundamentals of soil behavior. Third Edition ed. John Wiley & Sons, Inc., Hoboken, New Jersey.

Monroy, R., Zdravkovic, L. and Ridley, A. 2010. Evolution of microstructure in compacted London Clay during wetting and loading. Geotechnique, **60**, 105-119, doi: 10.1680/geot.8.P.125.

Moore, D.M. and Reynolds, R.C., Jr. 1997. X-ray diffraction and the identification and analysis of clay minerals. Second Edition ed. Oxford University Press, New York.

Oda, M. 1972. Initial fabrics and their relations to mechanical properties of granular material. Soils and Foundations, **12**, 17-36.

Pestana, J.M. and Whittle, A.J. 1995. Compression model for cohesionless soils. Geotechnique, **45**, 611-631.

Phillips, T.L., Loveless, J.K. and Bailey, S.W. 1980. Cr (super 3+) coordination in chlorites; a structural study of ten chromian chlorites. American Mineralogist, **65**, 112-122.

Porter, S.C. 2007. Loess Records | China. *In*: Editor-in-Chief: Scott, A.E. (ed.) *Encyclopedia of Quaternary Science*. Elsevier, Oxford, 1429-1440.

Righi, D. and Meunier, A. 1995. Origin of clays by rock weathering and soil formation. *In*: Velde, B. (ed.) *Origin and Mineralogy of Clays*. Springer-Verlag, Berlin, 43-161.

Roberts, H.M., Muhs, D.R. and Bettis Iii, E.A. 2007. Loess Records | North America. *In*: Editor-in-Chief: Scott, A.E. (ed.) *Encyclopedia of Quaternary Science*. Elsevier, Oxford, 1456-1466.

Rogers, C.D.F., Dijkstra, T.A. and Smalley, I.J. 1994. Hydroconsolidation and subsidence of loess - studies from China, Russia, North-America and Europe. Engineering Geology, **37**, 83-113, doi: 10.1016/0013-7952(94)90045-0.

Rousseau, D.D., Derbyshire, E., Antoine, P. and Hatté, C. 2007. Loess Records | Europe. *In*: Editor-in-Chief: Scott, A.E. (ed.) *Encyclopedia of Quaternary Science*. Elsevier, Oxford, 1440-1456.

Schwertmann, U. and Taylor, R.M. 1989. Iron oxides. *In*: Dixon, J.B. & Weed, S.B. (eds.) *Minerals in Soil Environments*. Soil Science Society of America, Madison, Wisconsin.

Sun, J.M. 2002. Provenance of loess material and formation of loess deposits on the Chinese Loess Plateau. Earth and Planetary Science Letters, **203**, 845-859, doi: 10.1016/s0012-821x(02)00921-4.

Sun, Y., Lu, H.Y. and An, Z.S. 2006. Grain size of loess, palaeosol and Red Clay deposits on the Chinese Loess Plateau: Significance for understanding pedogenic alteration and palaeomonsoon evolution. Palaeogeography Palaeoclimatology Palaeoecology, **241**, 129-138, doi: 10.1016/j.palaeo.2006.06.018.

Tan, T.K. 1988. Fundamental properties of loess from northwestern China. Engineering Geology, **25**, 103-122.

Trask, P.D. 1932. Origin and environment of source sediments of petroleum. The Gulf Publishing Company, Houston, Texas.

Tu, X.B., Kwong, A.K.L., Dai, F.C., Tham, L.G. and Min, H. 2009. Field monitoring of rainfall infiltration in a loess slope and analysis of failure mechanism of rainfall-induced landslides. Engineering Geology, **105**, 134-150, doi: 10.1016/j.enggeo.2008.11.011.

Wang, M., Bai, X.-h. and Yang, J. 2010. Method of Specimen Preparation for Collapsible Loess Microstructure Research. Journal of Taiyuan University of Technology, **41**, 283-286.

Xu, Z., Lin, Z. and Zhang, M. 2007. Loess in China and loess landslides. Chinese Journal of Rock Mechanics and Engineering, **26**, 1297-1312.

Yuan, Z.X. and Wang, L.M. 2009. Collapsibility and seismic settlement of loess. Engineering Geology, **105**, 119-123, doi: 10.1016/j.enggeo.2008.12.002.

Zárate, M.A. 2007. Loess Records | South America. *In*: Editor-in-Chief: Scott, A.E. (ed.) *Encyclopedia of Quaternary Science*. Elsevier, Oxford, 1466-1479.

Zhan, W. and Guggenheim, S. 1995. The dehydroxylation of chlorite and the formation of topotactic product phases. Clays and Clay Minerals, **43**, 622-629.

Zhang, G., Germaine, J.T., Whittle, A.J. and Ladd, C.C. 2004. Soil structure of a highly weathered old alluvium. Geotechnique, **54**, 453-466, doi: 10.1680/geot.2004.54.7.453.

Table 1. Some basic physical and index properties of the loess sample.

Property	Value	Determination method
Natural water content, w_n	20.3%	ASTM D 2216
Liquid limit, w_L	30.0%	ASTM D 4318
Plastic limit, w_P	19.3%	
Plasticity index, I_P	10.7%	
Specific gravity, G_s	2.70	ASTM D 854
In situ void ratio, e_0	1.19	Not available
In situ density, γ_0	1.52 Mg/m^3	Not available
Clay fraction	19.4%	ASTM D 2217 ASTM D 422
Silt fraction	77.0%	
Sand fraction	3.6%	
Median particle size, D_{50}	12.0 μm	
Soil classification	CL	ASTM D 2487

Table 2. Summary of the mineralogical composition of the studied loess.

Classification	Name	Ideal formula
Non-clay minerals	Quartz	SiO_2
	Albite (a plagioclase feldspar)	$NaAlSi_3O_8$
	Muscovite	$KAl_2(Si_3Al)O_{10}(OH,F)_2$
	Calcite (both primary and secondary)	$CaCO_3$
Clay minerals	Nimite	$(Ni,Mg,Fe^{2+})_5Al(Si_3Al)O_{10}(OH)_8$
	Clinochlore (only in the <2 μm fraction)	$(Mg,Fe^{2+})_5Al(Si_3Al)O_{10}(OH)_8$

Table 3. Major elements detected by EDXS from the interested spots in the loess.

Description	Sample V		Sample H	
	Spots	Elements	Spots	Elements
Dark zone	1	C, O, Cl	H4	C, Cl
Particles	2, 3, 7, 8, 12, 15, 16	C, O, Mg, Ca, Na, Al, Si, K, Ni, F, Fe	H1, H5, H6, H10, H13, H17	Si, O except H5 (O, Na, Al, Si)
Strip-like particles	10	C, O, Mg, Al, Si, K, Fe	H7, H11	Si, O
Particle tips	11, 17	C, O, Mg, Al, Si, K, Fe	H8	Si, O
Bright particle boundaries	4, 9, 13	C, O, Na, Mg, Al, Si, K, Ca, Fe	H2, H3, H9, H16	C, O, Al, Si, K, Ca, Ti, Fe
Zones between particles	6, 14, 18	C, O, F, Na, Mg, Al, Si, P, K, Ca, Fe, Cr	H12, H14, H15, H18, H19	Si, Ca, Fe, O, Al
Clay aggregate	5	C, O, Na, Mg, Al, Si, P, K, Ca, Fe		

Note: The element Pt is not included because it is from the artificially introduced coating layer on samples.

Figure captions

Figure 1. (a) Major occurrence of the Loess Plateau in China and the sampling location at an excavation site (Latitude: 34.317849^{o}, Longitude: 108.936811^{o}) in Xi'an; (b) Soil profile at the sampling site.

Figure 2. The plasticity chart showing the classification of different loesses (Gibbs and Holland 1960) and the studied loess.

Figure 3. Results of the double oedometer tests showing the compression curves obtained from a specimen with natural water content and an inundated specimen as well as the collapse index.

Figure 4. XRD patterns of loess samples subjected to different treatment (M = muscovite, N = nimite, Q = quartz, A = albite, Ca = calcite, C = clinochlore).

Figure 5. SEM micrographs showing the overall structure of the loess: (a) and (b) Sample V; (c) and (d) Sample H. Note (d) is a magnified view of the box in (c). B1 and D2: metastable particle chains; C1, C2, and C3: clay-silt mixture aggregates; D1: a silt particle with clay coating.

Figure 6. SEM micrographs showing the microstructure of the loess: (a) Sample V; (b), (c), and (d) Sample H. Note (c) is a magnified view of the box in (b), and (d) is a magnified view of the box in (c). M: muscovite particles.

Figure 7. SEM micrographs showing unstable contacts and a pure clay aggregate. Note that clay coating around Particles P1 and P3. A1: a pure clay aggregate of 30-40 μm in size; B1: an unstable particle contact.

Figure 8. Comparison of (a) the original SEM micrograph selected for image analysis and (b) the processed image with identified and isolated silt particles.

Figure 9. Statistical distributions of (a) the ECD, (b) sphericity, (c) HS circularity, and (d) elongation of the analyzed silt particles

Figure 10. SEM micrographs showing the interested spots analyzed by EDXS.

Figure 11. Selected EDXS spectra showing the elemental compositions of interested spots shown in Figure 10.

Figure 12. A conceptual microstructural model of a four-tired hierarchy. Insets (a) and (b) show a silt particle with clay coating and clay-silts aggregates, respectively.

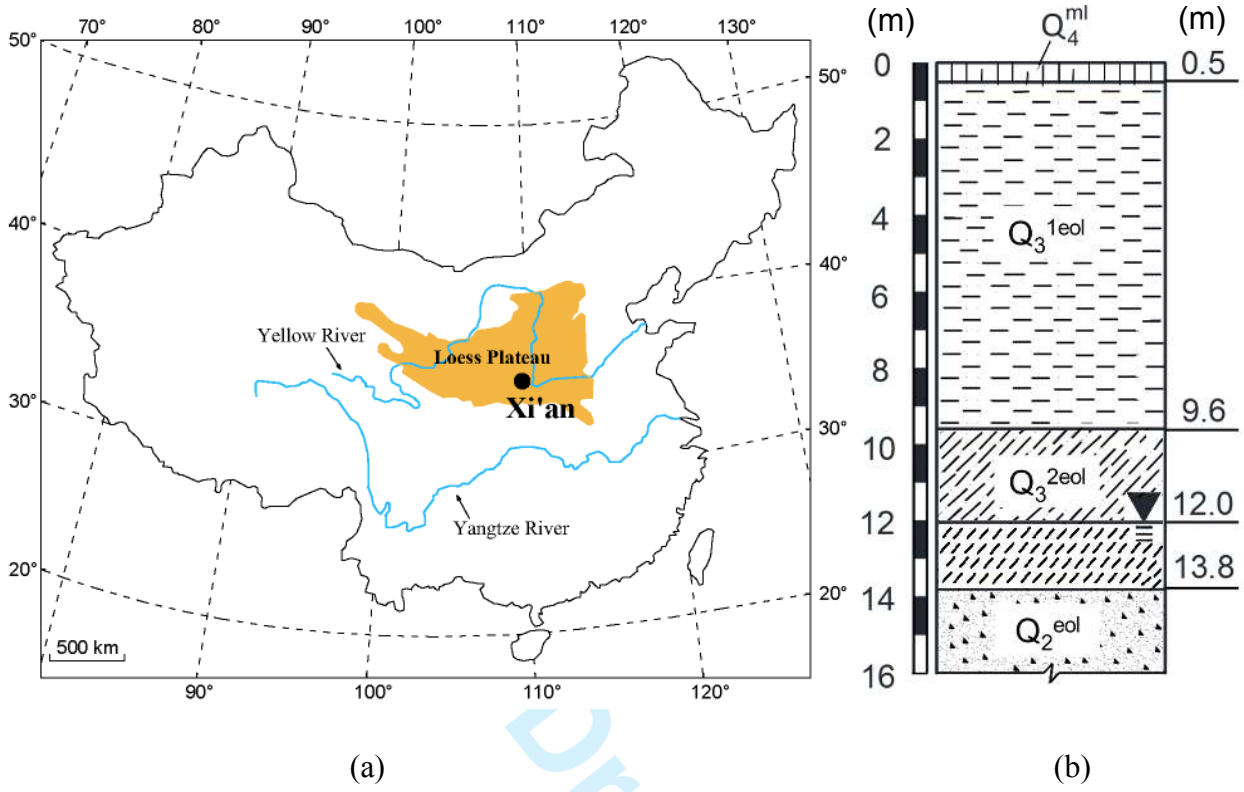

(a) (b)

Figure 1. (a) Major occurrence of the Loess Plateau in China and the sampling location at an excavation site (Latitude: 34.317849°, Longitude: 108.936811°) in Xi'an; (b) Soil profile at the sampling site.

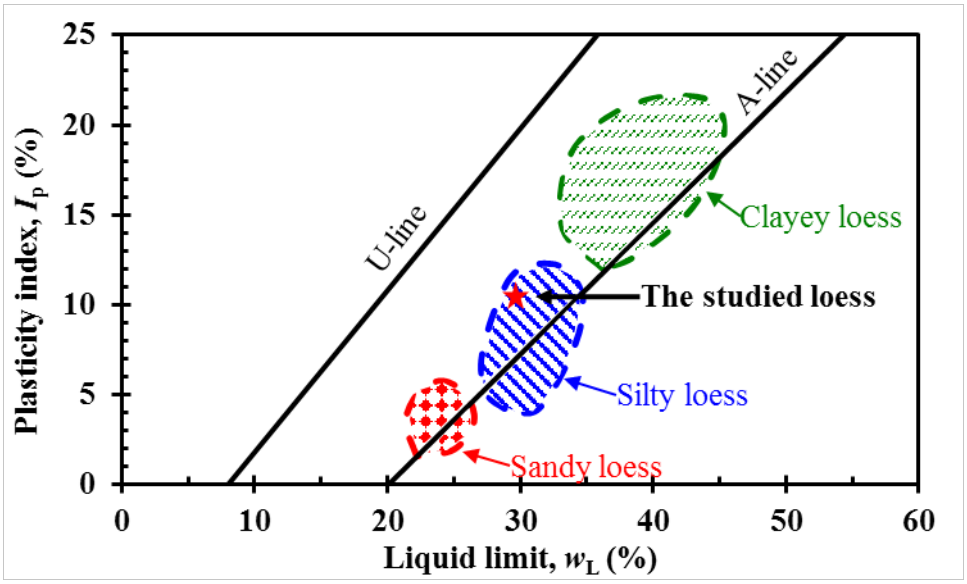

Figure 2. The plasticity chart showing the classification of different loesses (Gibbs and Holland, 1960) and the studied loess. *U*-line: $I_P = 0.9\ (w_L - 8)$; *A*-line: $I_P = 0.73\ (w_L - 20)$.

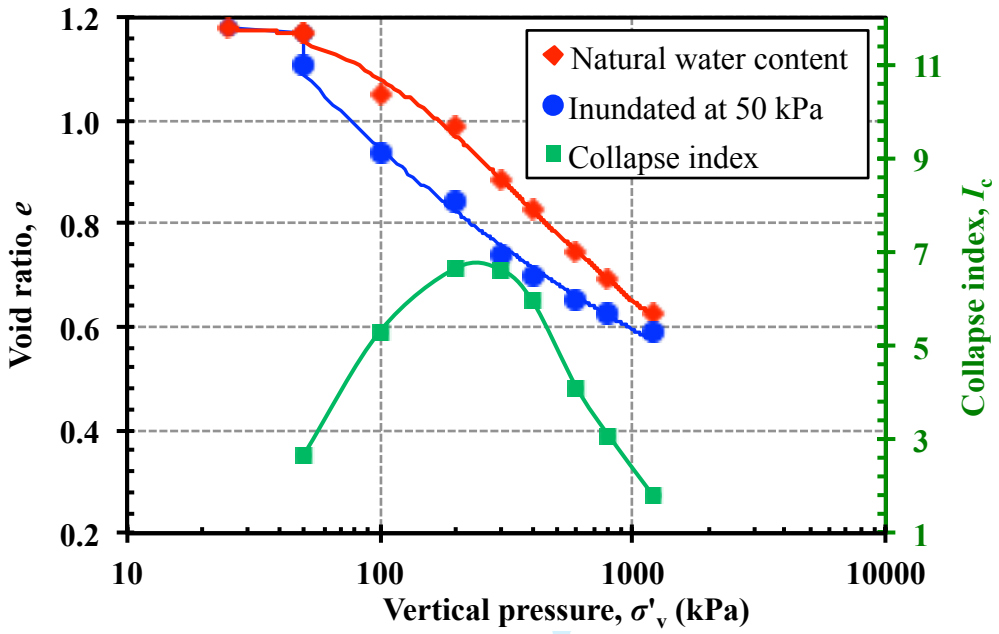

Figure 3. Results of the double oedometer tests showing the compression curves obtained from a specimen with natural water content and an inundated specimen as well as the collapse index.

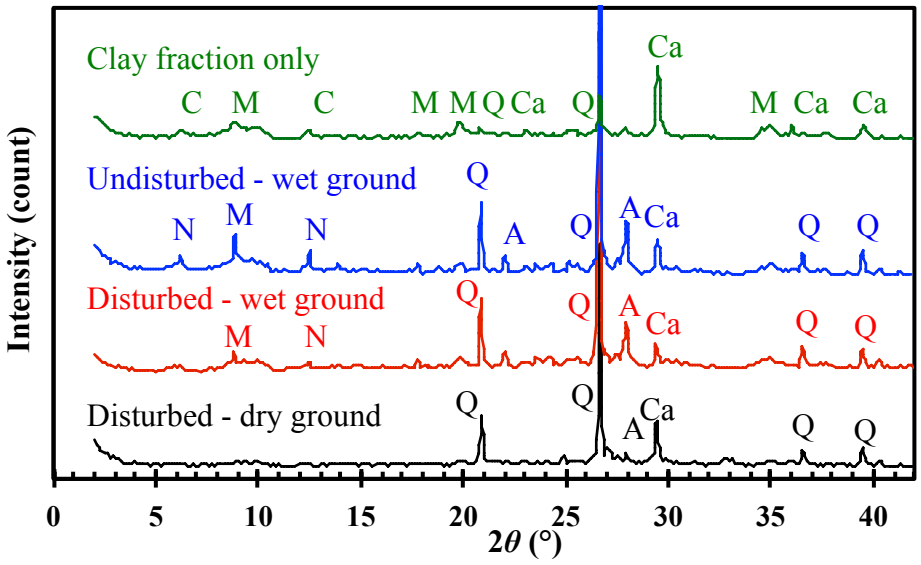

Figure 4. XRD patterns of loess samples subjected to different treatment (M = muscovite, N = nimite, Q = quartz, A = albite, Ca = calcite, C = clinochlore).

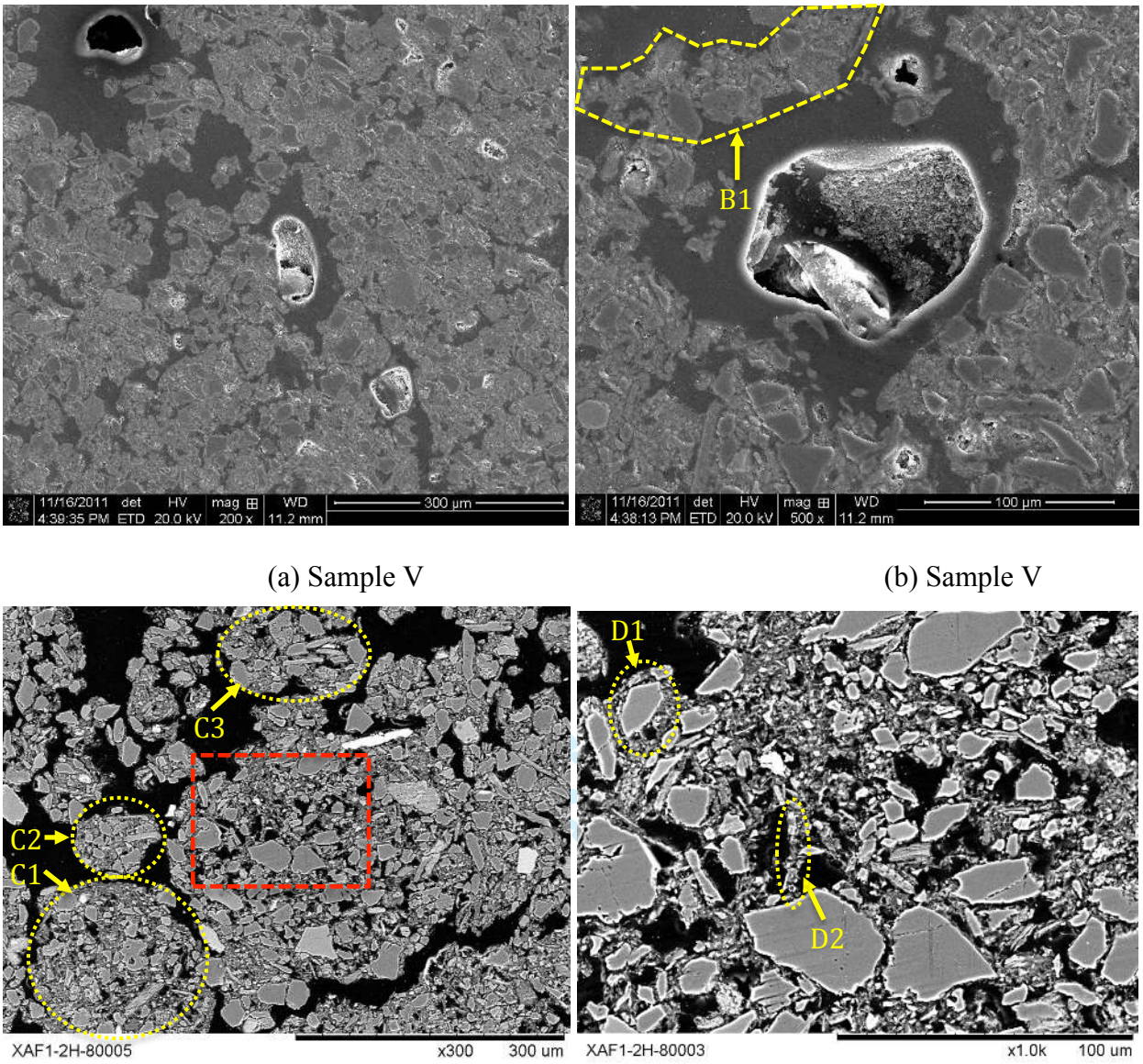

(a) Sample V (b) Sample V

(c) Sample H (d) Sample H

Figure 5. SEM micrographs showing the overall structure of the loess: (a) and (b) Sample V; (c) and (d) Sample H. Note (d) is a magnified view of the box in (c). B1 and D2: metastable particle chains; C1, C2, and C3: clay-silt mixture aggregates; D1: a silt particle with clay coating.

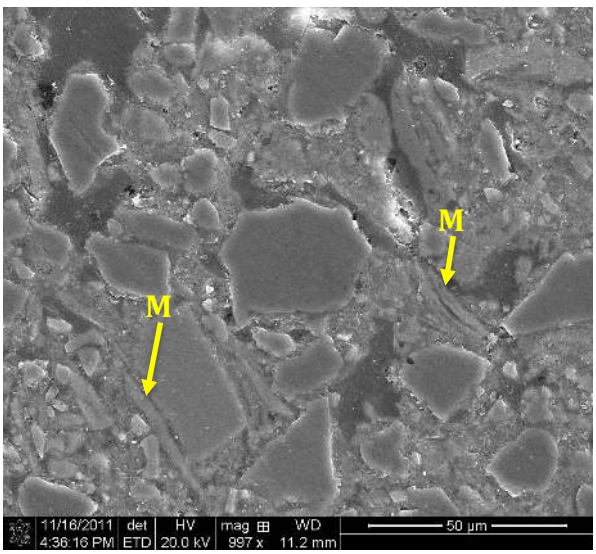

(a) Sample V: clay filling between silt particles

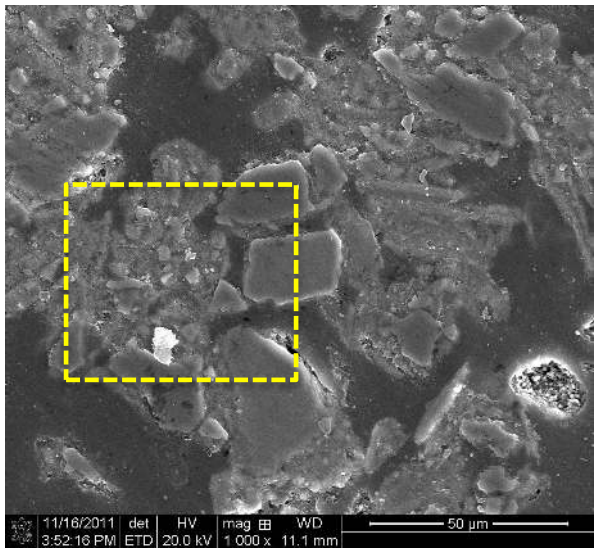

(b) Sample H: clay bridging

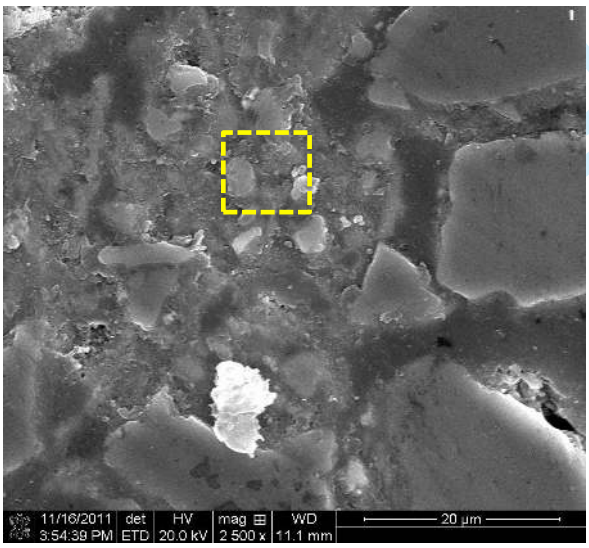

(c) Sample H: clay-silt aggregate

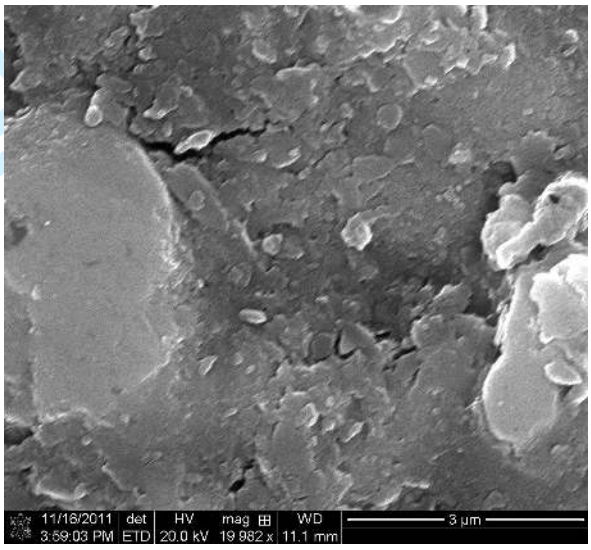

(d) Sample H: clay cementation

Figure 6. SEM micrographs showing the microstructure of the loess: (a) Sample V; (b), (c), and (d) Sample H. Note (c) is a magnified view of the box in (b), and (d) is a magnified view of the box in (c). M: muscovite particles.

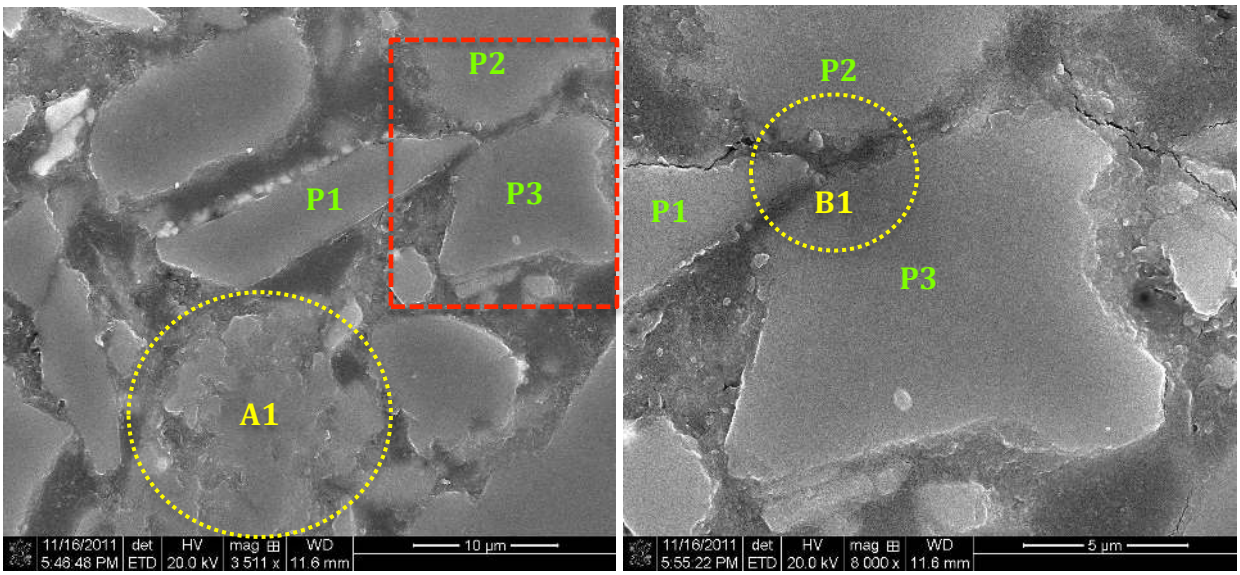

(a) Unstable contacts and a clay aggregate (b) A magnified view of the box in (a)

Figure 7. SEM micrographs showing unstable contacts and a pure clay aggregate. Note that clay coating around Particles P1 and P3. A1: a pure clay aggregate of 30-40 μm in size; B1: an unstable particle contact.

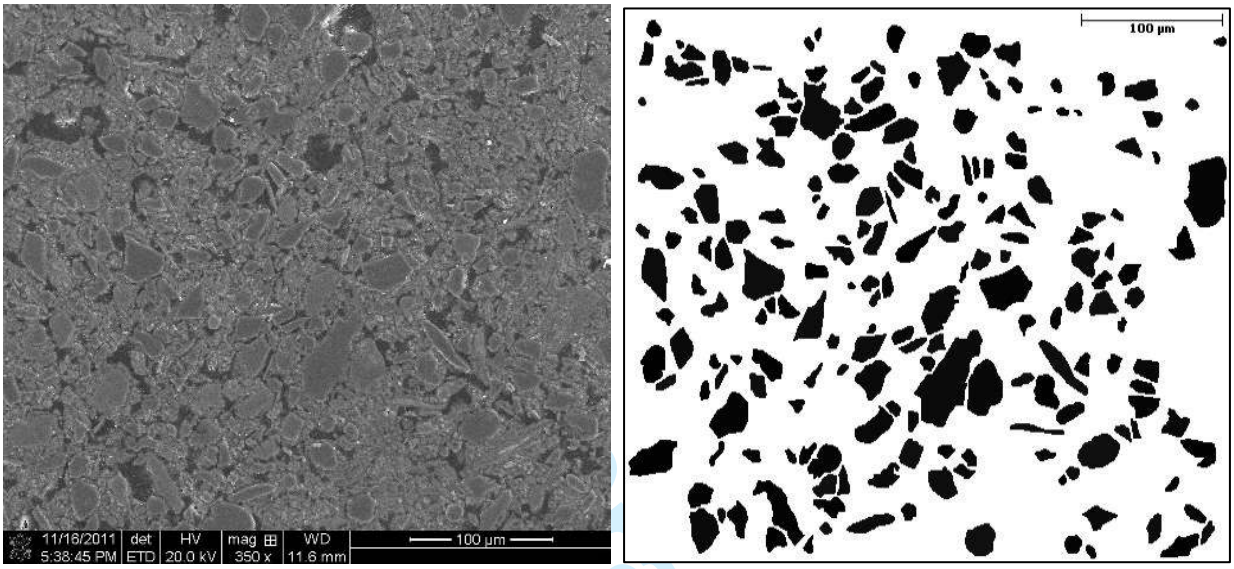

(a) (b)

Figure 8. Comparison of (a) the original SEM micrograph selected for image analysis and (b) the processed image with identified and isolated silt particles.

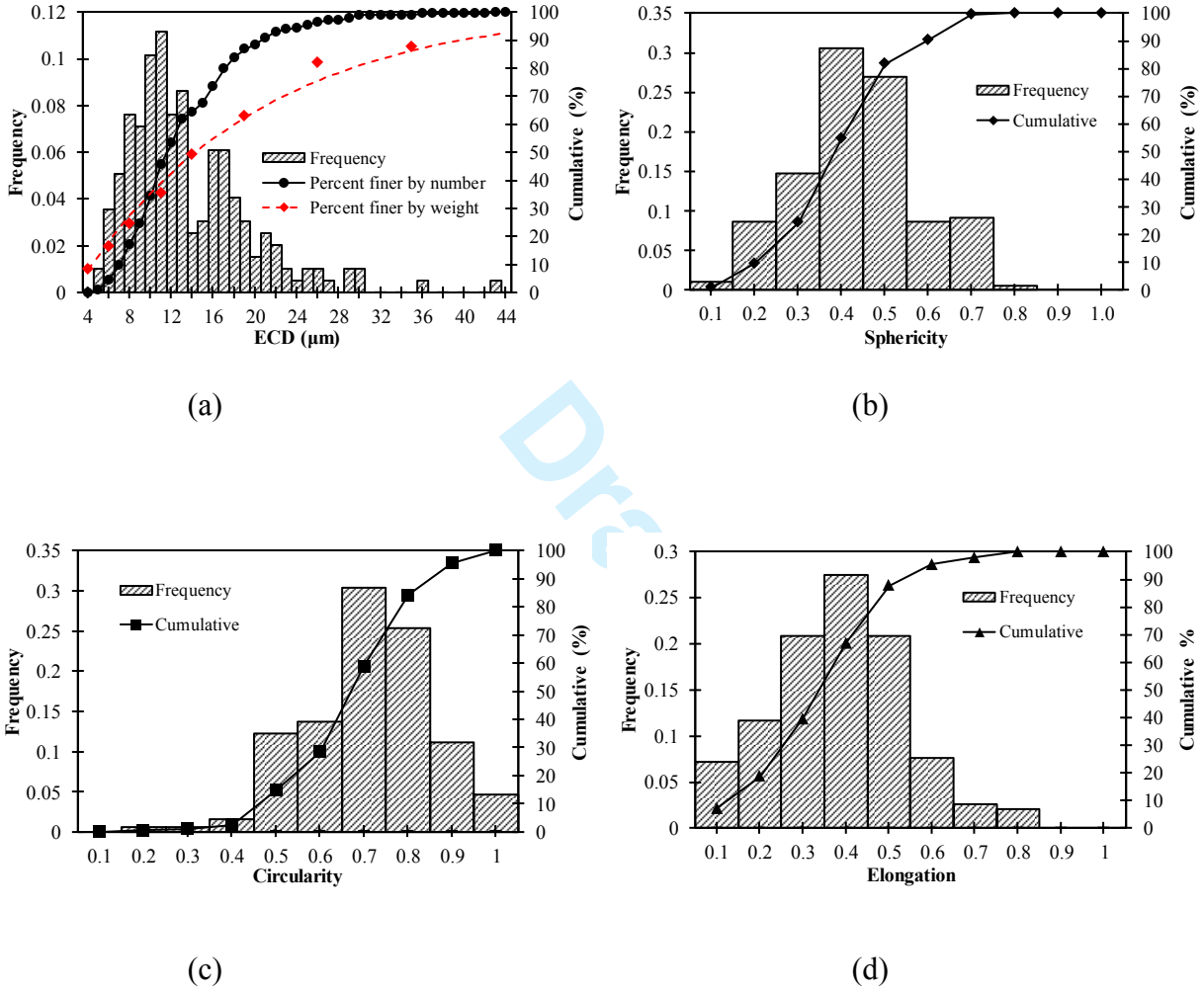

Figure 9. Statistical distributions of (a) the ECD, (b) sphericity, (c) HS circularity, and (d) elongation of the analyzed silt particles

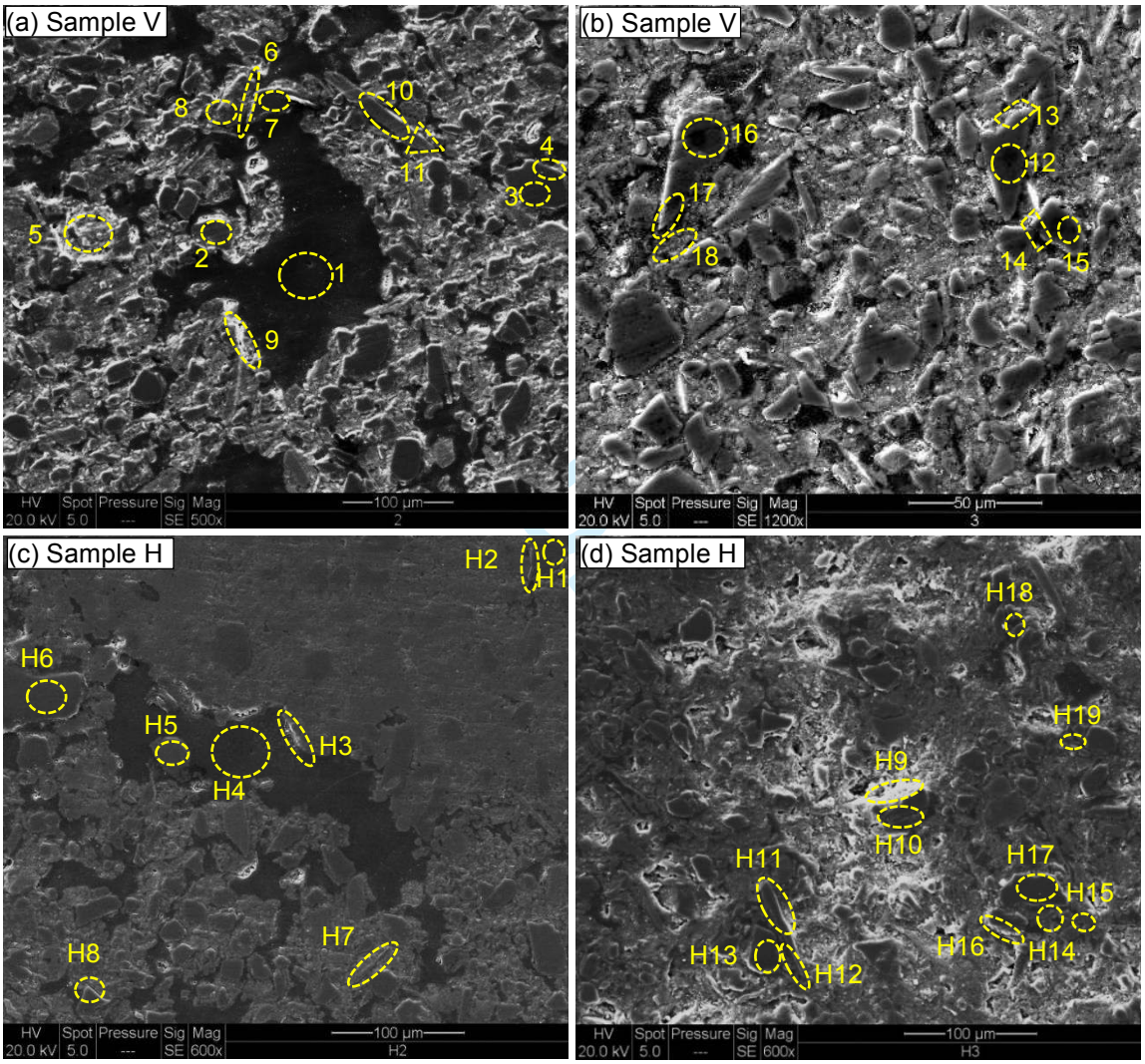

Figure 10. SEM micrographs showing the interested spots analyzed by EDXS.

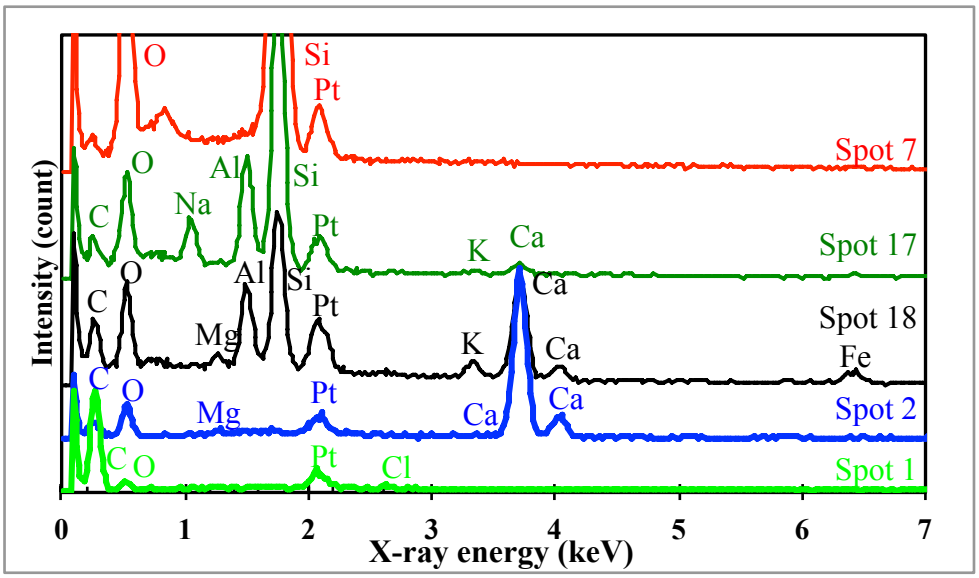

(a) Sample V

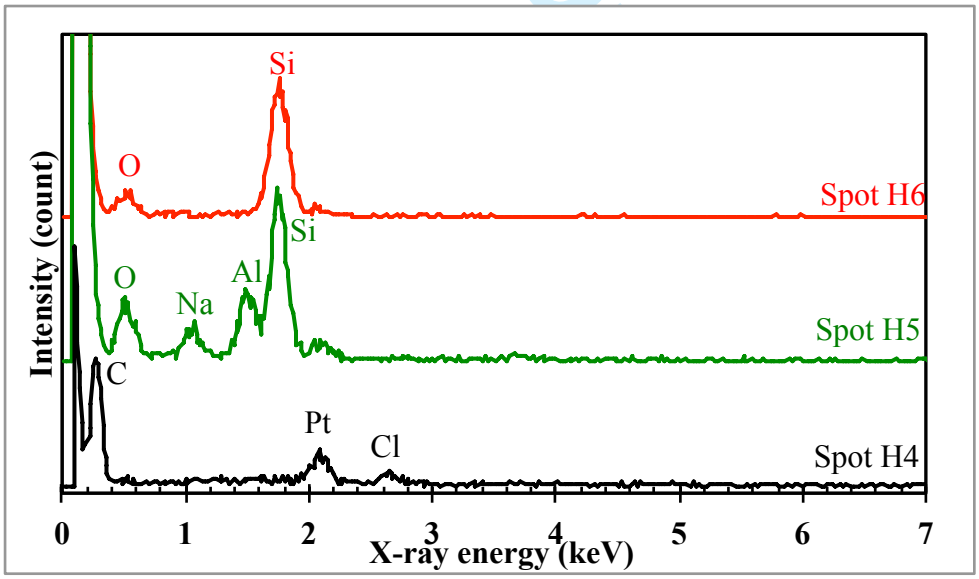

(b) Sample H

Figure 11. Selected EDXS spectra showing the elemental compositions of interested spots shown in Figure 10.

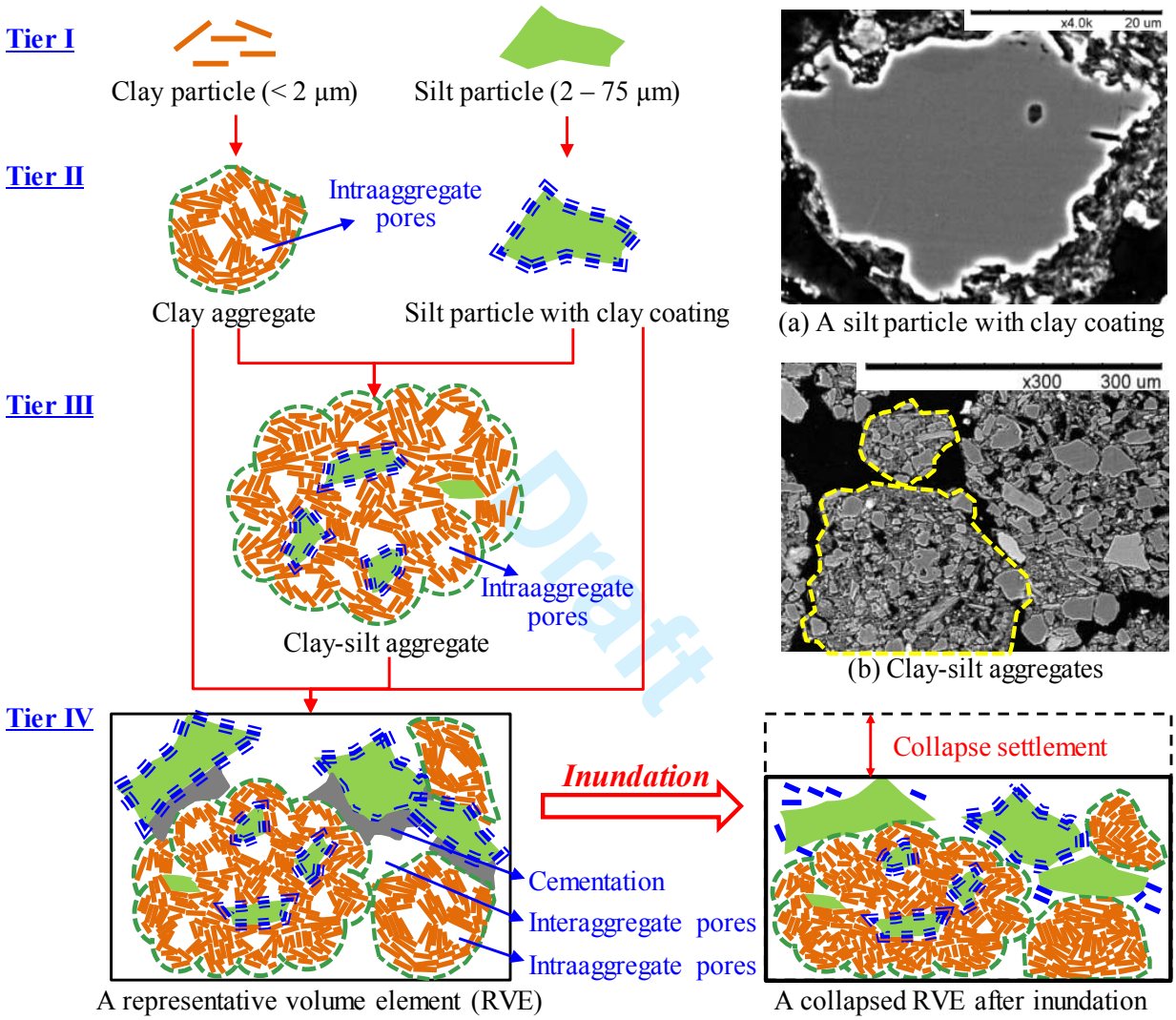

Figure 12. A conceptual microstructural model of a four-tired hierarchy. Insets (a) and (b) show a silt particle with clay coating and clay-silts aggregates, respectively.